A Discretely Assembled Walking Motor

Will Langford[1*] and Neil Gershenfeld[1]

***Abstract*—We introduce a discrete approach to robotic construction that enables the integration of structure, mechanism, and actuation and offers a promising route to on-demand robot fabrication. We demonstrate this with the assembly of a centimeter-scale Discretely Assembled Walking Motor (DAWM) capable of producing large scale linear or rotary motion from five millimeter-scale part types. The five part types each embody a limited capability including rigid (strut and node), flexural, magnetic, or coil. Through their arrangement in a three-dimensional lattice, we demonstrate the assembly of actuated mechanical degrees-of-freedom in a useful small-scale machine. This work extends prior research in discrete material systems with the inclusion of flexural and actuation components. Actuation is accomplished with the use of voice coil actuator components that produce up to 42mN of force and strokes of 2mm. This performance compares well with other millimeter scale actuators and provides sufficient force to lift 28 connected nodes in our assembled lattice, or 7 other actuator components. DAWM is capable of stepping at rates of up to 35Hz, resulting in velocities of up to 25mm/s. Multiple DAWM systems can be stacked to add force and can be driven in-phase or out-of-phase to produce intermittent or continuous force, respectively. This approach to robot fabrication discretizes robotic systems at a much finer granularity than prior work in modular robotics and demonstrates the possibility of assembling useful small-scale machines from a limited set of standard part types.**

I. INTRODUCTION

The design and fabrication of robots today can be expensive, inflexible, and time-consuming, often requiring the integration of a variety of parts, each made using separate and unrelated processes and with no standard assembly interface. The assembly and integration of these parts often represents a bottleneck in both the time and flexibility of the fabrication of a novel robotic system and as a result, recent research has looked for ways to fabricate robots in a more integrated way [1] [2].

One way this assembly bottleneck has been addressed is with modular and reconfigurable components. Modular robotic systems integrate a number of capabilities such as actuation, communication, and control within every building block, enabling configuration and reconfiguration to suit a particular task. While these systems illustrate the universality of modular construction methods, the resulting modules tend to be relatively complex, involve dense integration of the various embedded functions, and are expensive to fabricate in volume [3]. As a result they have typically found limited use outside of the research lab.

The approach we introduce is based on discretely assembled "digital" materials. Digital materials are based on a discrete set of parts, which are reversibly joined with a discrete set of relative positions and orientations [4]. These properties allow global geometries to be determined from local constraints, assembly errors to be detected and corrected, heterogeneous materials to be joined, and disassembly and reuse rather than disposal [5]. Digital materials have been used to produce the highest reported modulus ultralight materials [6], shape morphing structures with the use of rigid and flexural parts [7], as well as electronic structures with the addition of conductive and insulating parts [8] [9].

We extend the space of digital materials here with the introduction of large-displacement flexural parts and actuation elements and demonstrate the assembly of electromechanical systems from just five part types. This approach builds systems with integrated structure, mechanisms, and actuation in a way that can be incrementally extended and modified. Standardizing the assembly interfaces between parts and simplifying the assembly process, to require just a single vertical motion, means the assembly process can more closely resemble a digital fabrication workflow. This ability to assemble integrated robotic systems from a small library of heterogeneous parts points towards the possibility for on-demand fabrication of a wide range of robots.

We demonstrate the assembly of long range continuous motion from a small set of discrete parts by means of a Discretely Assembled Walking Motor (DAWM) (Fig. 1). The DAWM system helps answer questions about the viability of this assembly method for the fabrication of robotic systems and provides a test bed to quantify the performance of discretely assembled systems including the kinematics, dynamics, and coordination of multiple degrees of freedom.

In the following sections we detail the part and lattice geometry used as a basis for this work, the flexural parts that enable the assembly of mechanisms, the design and characterization of actuation elements, their integration in the DAWM system for linear and rotary motion, and the possibility to scale this design to other length scales.

II. PART AND LATTICE GEOMETRY

We assemble digital material structures from repeated building block parts arranged in a rectangular lattice framework (Fig. 1). Nodes of the lattice are assembled from four identical two-dimensional parts connected at their edges. Nodes are connected by struts, which are either a simple two-dimensional part or a functional part such as a flexural degree-of-freedom or actuator.

The parts interlock through press-fit connections. The dimension of these slots is tuned to balance the force of insertion required during assembly with the mechanical and electrical

[1] Massachusetts Institute of Technology, Center for Bits and Atoms
[*] Corresponding author: will.langford@cba.mit.edu
This work was funded by Army Research Office (ARO) award W911NF-16-1-0568, and the Center for Bits and Atoms consortium.

978-1-7281-0948-0/19/$31.00 ©2019 IEEE

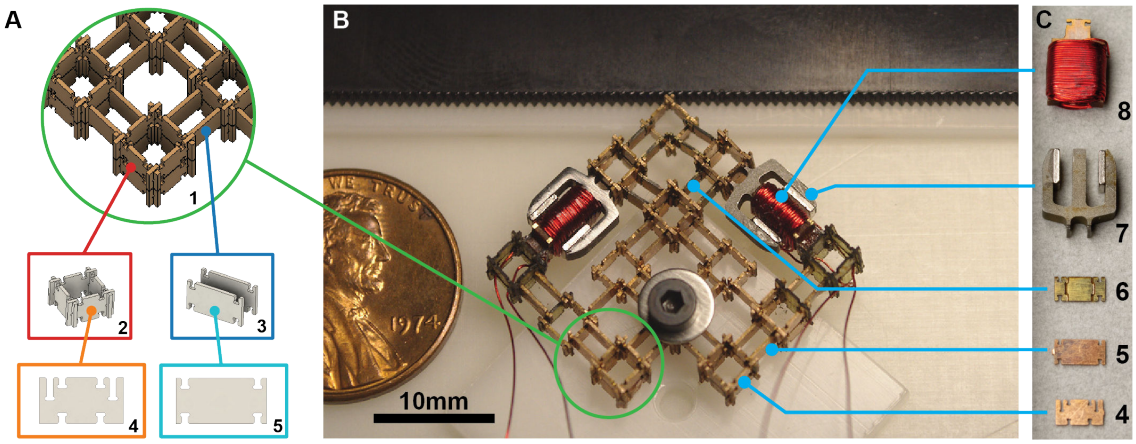

Fig. 1. An overview of the walking motor assembled from five part types. (A) The lattice decomposition into two-dimensional parts. Node parts (4) are first assembled into nodes (2) which are then connected with struts (5) arranged in parallel (3). (B) A single-layer walking motor configured to produce linear motion. (C) The five part types that go into the walking motor: node parts (4), rigid struts (5), dual-hinge struts (6), magnetic core (7), and voice coil (8).

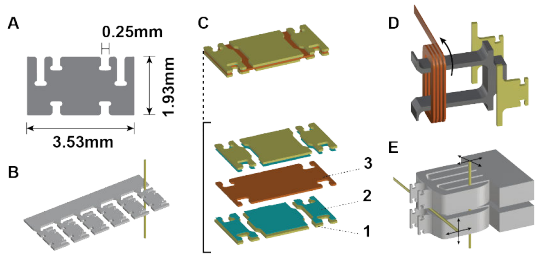

Fig. 2. Part production techniques used in prototyping. Dimensioned node part (A) is cut with wire-EDM (B). Parts with flexural hinges (C) are fabricated by laminating layers of brass (1), B-staged adhesive (2), and Kapton (3). Coil parts are made by winding wire around a mandrel (D). Magnetic cores are made with two orthogonal wire-EDM cuts (E).

reliability of the connection [8]. The parts are designed for automated assembly such that all of the interlocking connections are made in the vertical direction, enabling assembly with a simple single degree-of-freedom vertical motion.

The basic part types are two-dimensional so that they can be mass-produced in a range of materials and with a wide range of processes. While this assembly method may be applicable at a number of length scales, we have focused on the development of these parts at the millimeter scale. The parts shown here are 3.53mm in their longest dimension, are 254μm thick, and their smallest feature size is 200μm (Fig. 2).

By embedding degrees of freedom in the parts themselves, we can assemble mechanisms and linkages (Fig. 3). Flexural parts are fabricated using a multi-layer laminate technique referred to as PC-MEMS (printed circuit MEMS) or SCM (smart composite microstructures) [10] [11] [12]. This technique enables the fabrication of hinges that are highly compliant about the hinge-axis but stiff off-axis. In this way, the flexural hinges act similarly to conventional macroscopic pin-joints but have the advantage of having virtually no backlash about their axis of rotation.

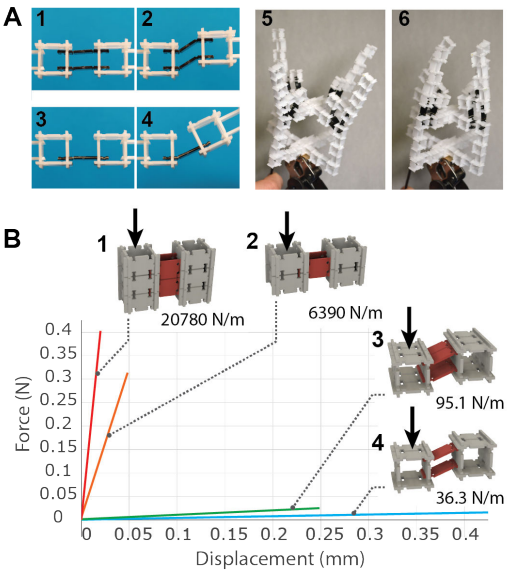

Fig. 3. Mechanisms are assembled from parts with flexural degrees of freedom. Two common mechanism motifs (A) are parallelogram linkages (1)(2) and a single-hinge rotary joint (3)(4). These are combined to assemble a gripper (5)(6). The mechanisms exhibit a high degree of compliance on-axis while remaining stiff off-axis (B).

The flexural parts are made from layers of brass (100 μm thick) and Kapton (25 μm thick), and joined with two layers of B-staged Pyralux adhesive (12.5 μm thick) as pictured in Fig. 2. This construction produces a hinge joint that is much more compliant about its rotation axis (28.9 mNmm/rad) than off-axis (9700 mNmm/rad). Similarly, a parallelogram linkage assembled from two degree-of-freedom struts measures 36.3 N/m on-axis and 6600 N/m off-axis.

A. Actuator Component Design and Characterization

At the millimeter scale, a number of actuation techniques can be used to drive these mechanisms, including piezoelectric

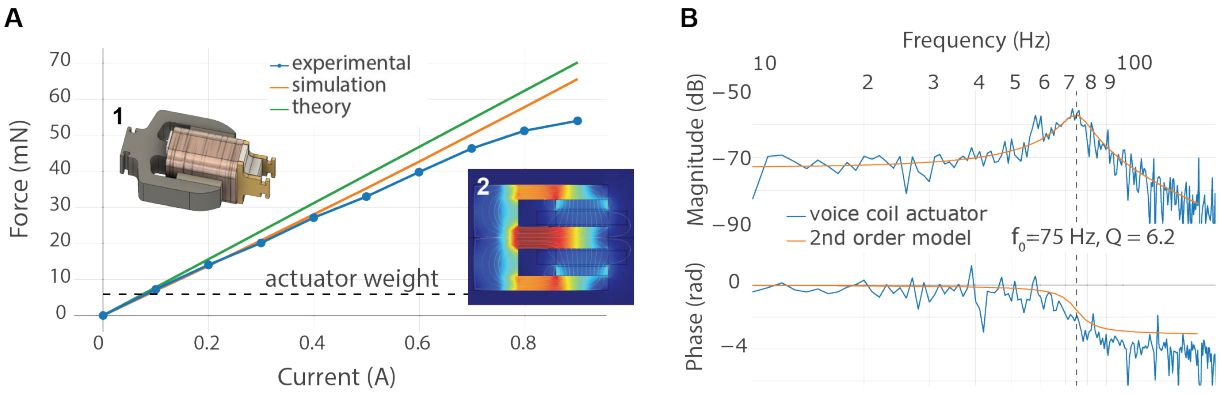

Fig. 4. Actuator characterization. (A) The results of static testing and comparisons with theoretical and numerical modeling. (B) The results of dynamic testing showing a natural resonant frequency of the actuator and mechanism combination of 75Hz.

bending actuators [13], dielectric elastomer actuators [14], shape-memory alloy actuators [15], and electromagnetic actuators [16].

We use electromagnetic Lorentz force (voice coil) actuation for its ability to produce constant force over long ranges. Electromagnetic actuators are used extensively at macro-scales but are less common at smaller scales because of energy-density scaling. However, considering improved current capacities at smaller scales and with the use of permanent magnets, use of electromagnetic actuators can be extended down to smaller sizes [17]. Relative to other electromagnetic actuators, Lorentz force actuators are able to produce a constant force (proportional to current) over a longer stroke and at a high-bandwidth. Additionally, there is no attractive force between the magnet core and coil, which reduces the demands on the mechanisms that constrain the coil's motion.

The actuator components span two cells of the lattice geometry and is pictured in Fig. 4. This reduces the volumetric overhead associated with the integration of the coil and the magnetic core and means the force producing components can take up a larger portion of the overall volume. We designed the actuators to maximize their force over a 2 mm stroke. Like all other parts in this assembly system, the actuator components are designed to be vertically assemble-able and interface with the lattice using the same press-fit connections. Additionally, while the actuator components are more geometrically complex than the basic structural parts, they are still designed to be relatively easily mass produced. Coils of this size are regularly produced in large quantities, relatively inexpensively using surface mount inductor coil production techniques [18]. For prototyping we fabricate the parts using laminate methods, wire EDM, and semi-automated coil winding (Fig. 2).

We modeled the actuator component using both magnetic circuit analysis and COMSOL multiphysics simulation software and verified this modeling with the physical testing detailed below. The static and dynamic performance of the actuator component is summarized in Table I.

1) Static Characterization: We tested the actuators both statically and dynamically. During static testing, we varied the current through the actuator coils and measured the resulting output force. The results show that the force of the actuator is linear with current and closely matches both analytical and numerical simulations (Fig. 4). Because the models do not account for static friction or irregularities in the winding of the coil, they tend to over-predict the performance of the actuator. The analytical model also neglects leakage flux, which is unrealistic given the size of the air gap in the actuator.

TABLE I
CHARACTERISTICS OF THE ACTUATOR COMPONENT

Coil Turns	75
Max. Continuous Current	0.6 A
Max. Continuous Current Density	24.2 A/mm^2
Force (blocked mid-stroke)	42 mN
Stroke (no load)	2.1 mm
Resonance (incl. parallelogram linkage)	75 Hz
Overall Mass	511 mg
Energy Density	86 J/g

In Fig. 4, beyond 700 mA, the actuator force becomes sub-linear with current. This is likely a result of high temperatures in the coil affecting the effective flux density supplied by the magnets. We take 600mA as the actuator's maximum steady state operating current, at which it reaches a temperature of 67 °C and produces an output force of 42mN. Taking into account the cross-sectional area of a single wire turn, this represents a current density of 24.2 A/mm^2, which is more than two times greater than the recommended maximum current density for macroscopic electromagnetic actuators [19]; this is possible because of the relative scaling of surface area and volume, which allows better heat transfer out of the coil [17]. The 42mN of output force is enough to lift 28 nodes of the lattice or 7 other actuator components, which is sufficient to produce useful motions and forces in discretely assembled machines with multiple degrees of freedom.

2) Dynamic Characterization: To measure the dynamic performance of the actuator, we supply a pseudo-random voltage to the actuator and use a high-speed camera to measure its response. The coil component of the actuator is rigidly

fixed while the magnetic component is constrained by an assembled parallelogram flexure linkage, which approximates linear motion for small displacements. Dividing the frequency response of the output displacement by that of the input voltage, results in the transfer function that describes how the output relates to the input over a range of frequencies. This data, presented in Fig. 4, is described well by a second-order spring mass damper model with a 75 Hz natural frequency and a quality factor of 6.2. This model is useful in predicting the performance of the actuated system over a range of frequencies and gives an estimate of the bandwidth of the actuator and flexure combination.

3) Comparison to other millimeter-scale actuators: The actuator component developed here compares well against other millimeter-scale actuators that have been recently reported in research. We compiled data regarding actuator force, mass, stroke, and bandwidth and plot the normalized actuator force (per weight) against maximum stroke (Fig. 5). Wherever possible we include the mass of the whole actuator (stator and mover) as well as the mass of the motion constraint.

The actuator component developed in this work has the highest normalized force (blocked force per weight) of any of the comparably sized electromagnetic actuators presented here [20][16][21][22][23][24]. Piezoelectric [13][25] and electrostatic [26][27] actuators produce more force per mass but are more limited in their available stroke. We discuss possible methods to increase the performance of the actuator in the conclusion.

III. SYSTEM INTEGRATION

We built a Discretely Assembled Walking Motor (DAWM) to demonstrate the integration of structure, mechanism, and actuation. The DAWM system takes small cyclical steps to produce long range motion of a sliding or rotating element. This principle of locomotion is most commonly used with piezoelectric actuators [28] for applications such as nanometer-precision stages [29] and focusing motors in DSLR cameras

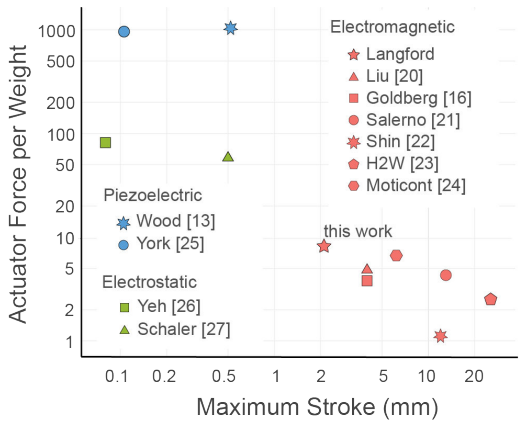

Fig. 5. Comparison of normalized force versus stroke with other research and commercial millimeter-scale actuators.

[30]. Here, we use the voice coil actuator components developed for our assembled structures to enable the same kinds of motion with larger displacements and lower voltages.

The walking motor is composed of five part types: structural nodes, rigid and dual-hinged struts, and magnetic and coil part types (Fig. 1). The two actuator components are oriented perpendicularly to one another and the output of the actuators is coupled to a motor tip through multiple four-bar parallelogram linkages, which distribute the two degrees of freedom at the tip into a single degree of freedom at each actuator. As the motor tip is driven cyclically, it engages with a grooved sliding or rotating element. In our design, the motor tip consists of a 0.5 mm cylinder which provides quasi-kinematic mating with the triangular grooves of the rotor. The triangular grooves are spaced 0.75 mm apart and correspond to a segment of the approximately circular trajectory of the motor tip. This geometry is designed to allow for the correction of motor-tip positioning errors within +/-0.15 mm. The motor works with a variety of different surfaces including ones that are smooth; however, the grooved surface employed here provides the highest repeatability.

A. Speed and Repeatability

We characterize the repeatability of the walking motor across a range of stepping frequencies, by taking 10 steps at each frequency and computing the average velocity at each. We sweep the frequency up and down, increasing and decreasing the step rate a number of times, to get a sample size of six at each tested frequency.

The results (Fig. 6) show good agreement to the predicted performance. Below 12 Hz, the difference between measured and predicted velocities is negligible. Between 12 Hz and 34 Hz, there is more variability in the relationship between step frequency and velocity with the largest standard deviation being 25% of the mean. However, the overall slope remains consistent with our predictions. This indicates that at the higher step-rates the motor is just as likely to take a double-step as it is to miss a step. We hypothesize that step variability occurs because the motion amplitude increases as the step-rate approaches the resonant frequency of the walking motor and causes the motor to occasionally skip a tooth. Beyond 35 Hz the velocity drops dramatically as the steps become very erratic and intermittent, indicating a maximum open loop speed of approximately 25 mm/s.

B. Force Additivity

To characterize the effects of phasing multiple walking motors, we measured the blocked force of a stacked two-layer walking motor while driving at a 1 Hz step rate to ensure sufficient resolution to resolve the full force profile (Fig. 6).

When the two motors are driven in phase, their peak force is approximately twice (70 mN) that of the single motor (30 mN). When the two motors are driven out of phase, they produce a more uniform force which varies between 20 mN and 50 mN. The magnitudes of these forces are on par with the maximum blocked force of the individual actuators themselves. In the

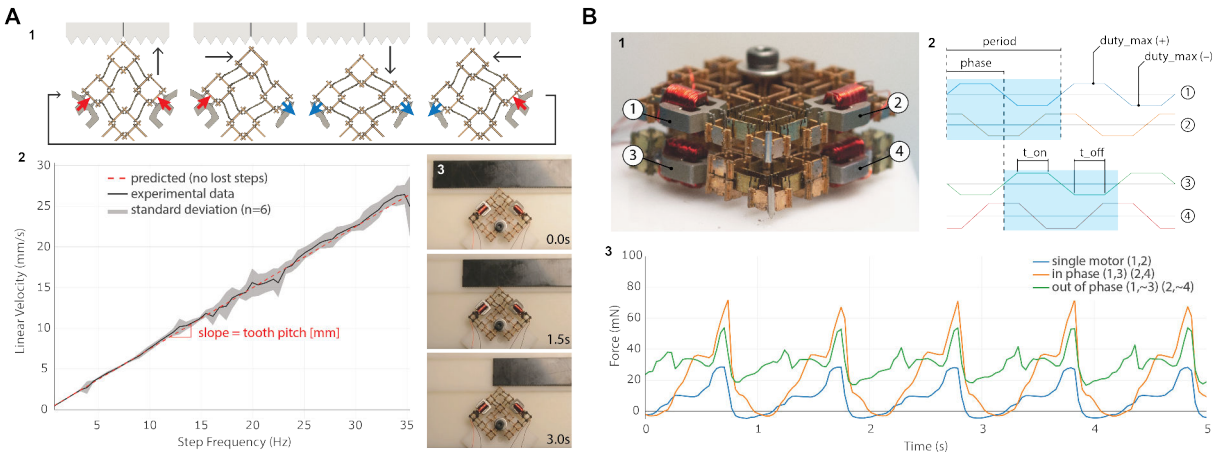

Fig. 6. Walking motor characterization. (A) Speed and reliability testing done on a single-layer walking motor illustrates the series of steps during one actuation cycle (1) as well as the progression of a slider over three seconds (3) and the resulting velocity of the mover/rotor (2). The force output of the walking motor (B)(1) driven by a trapezoidal waveform (2) out-of-phase and in-phase (3).

TABLE II
SCALING LAWS FOR VOICE COIL ACTUATION

Mass	s^3	Power	s^2
Current	s^1	Power Density	s^{-1}
Force	s^2	Force Density	s^{-1}
Bandwidth	s^{-1}	Efficiency	s^1
Energy Output	s^3	Energy Density	s^0

single motor case, 79% of the maximum blocked force of a single actuator is translated to the rotor at its peak force. In the two-motor case, 92% of the maximum blocked force of two single-actuators is translated to the rotor at its peak force.

C. Scaling

While we have focused development at the millimeter-scale, other application domains may be possible by scaling the constituent parts and assemblies. For example, with smaller micro-scale building block parts, applications requiring finer-grain resolution can be explored such as ingestible medical robots and dexterous microsurgical tools.

It is possible to project the performance of these assemblies to other length scales through a proportionality scaling analysis (Table II). We use the scale variable, s, to represent how a particular quantity scales, as is detailed in [17]. In our case, we assume that the actuation current can scale with a constant temperature rise (s^1), rather than constant current density (s^2), because surface area scales favorably with respect to volume. Based on this assumption, both power and force (as well as their respective densities) scale favorably to smaller length-scales. Furthermore, bandwidth also scales favorably, proportionally increasing for every shrink in size. Efficiency, however, suffers at smaller length scales and decreases proportionally with scale.

This points to the possibility of scaling this assembly approach down in length-scale. At some-point, however, the increase in bandwidth, force, and power density will be outweighed by the decrease in efficiency and will warrant a different type of actuation (for example, piezoelectric or electrostatic).

Assembly at smaller length scales is often complicated by decreased positioning accuracy and difficulties in part manipulation because of the scaling of surface forces relative to inertial ones. We expect our discrete assembly method to be more amenable to high throughput assembly at small scales because the assembly accuracy comes from the interlocking geometry of the parts, rather than a global positioning system, and the part-part interlocking forces can be tuned to enable reliable part placement. Prior work has shown that the degree of positioning error tolerance can be as high as 39% of the part spacing [8].

IV. CONCLUSIONS

We have shown that machines with integrated mechanisms and actuation can be assembled from a small set of building blocks. In particular, we developed five part-types that enable the assembly of a walking motor that converts small displacement cyclical motion into precise, long range linear and rotary motion at up to 25mm/s. We showed that by embedding flexural hinges in the part set, we can assemble compliant mechanisms that have high ratios of on- to off-axis compliance. Furthermore, we developed an actuator component, integrated in the same assembly framework, that produces enough force to lift seven times its own mass.

The maximum frequency of the DAWM system is 35Hz and is limited, in part, by the electronic drive circuitry. The actuator uses 34-awg wire, resulting in a low inductance coil (15μH) that experiences current ripple losses when driven directly by an H-bridge with insufficiently high frequency PWM (1kHz, in this case). Decreasing the wire diameter to 40-awg and increasing the PWM frequency to 31.25kHz would reduce the current ripple by 88% and the resulting dissipation by 70%,

potentially enabling actuation rates up to the 75Hz bandwidth of the actuator-flexure combination.

The actuation rate could be further increased by stiffening the flexure degrees-of-freedom. Our flexures were designed to be highly compliant to enable long strokes to suit a wide variety of applications. Given the electrical time constant of the actuator coils ($\tau = L/R = 100\mu s$), actuation rates of several hundreds or thousands of cycles per second should be possible at the expense of the actuator stroke. While the DAWM system has not been tested to fatigue, prior research has shown that the flexural hinges used here can be made to survive millions of cycles before failure [31].

To constrain the long range motions, we used commercially available ball bearings and sliding surfaces for rotary and linear motion, respectively. The part set developed here is capable of making linear and rotary constraints, but we made no attempt to use them to constrain the long range motions and leave that for future work. Additionally, we have not included discussion of methods to integrate circuitry, controls, and power storage within the same assembly framework. Prior work has shown the possibility of assembling circuitry, including active electronics in similar assembly systems [8][9]. Based on this, future work will involve the assembly of integrated robotic systems such as grippers, micro-positioners, and mobile robots with onboard power and control.

The regularity of the geometry in these assemblies lend themselves well to automated assembly. The work shown here was manually assembled, however prior work has shown the possibility of automating the assembly in a desktop process [9]. Prior assembly systems in this category have been able to leverage the interlocking nature of the discrete parts to assemble structures with a high degree of error tolerance [8].

In the same way that computers and digital technology rest on the ability of a small family of gates to evaluate arbitrary logical expressions [32], this work points to a small family of building blocks that enable the construction of arbitrary robotic capabilities. While the design and fabrication of robots today often requires the integration of many diverse and custom parts, by standardizing the part set through the development of discrete assembly workflows, we can take advantage of the same benefits inherent in computational universality and enable more flexible, inexpensive, and rapid design of robotic systems. The results reported here show the utility of even a limited standard part set and the opportunity for future work to extend the part set to encompass a full range of robotic capabilities.

REFERENCES

[1] S. Tibbits, "From Automated to Autonomous Assembly," *Architectural Design*, vol. 87, no. 4, pp. 6–15, 2017.

[2] J. Paik, "Soft robot design methodology for 'push-button' manufacturing," *Nature Reviews Materials*, pp. 1–3, 2018.

[3] Z. Butler and A. Rizzi, "Distributed and Cellular Robots," in *Springer Hanbook of Robotics*, pp. 911–920, 2008.

[4] G. A. Popescu, T. Mahale, and N. A. Gershenfeld, "Digital materials for digital printing," *NIP & Digital Fabrication Conference*, pp. 1–4, 2006.

[5] J. D. Hiller and H. Lipson, "Fully Recyclable Multi-Material Printing," *Solid Freeform Fabrication Symposium (SFF'09)*, 2009.

[6] K. C. Cheung and N. Gershenfeld, "Reversibly Assembled Cellular Composite Materials," *Science*, vol. 341, no. September, pp. 1219–1221, 2013.

[7] B. Jenett and K. C. Cheung, "BILL-E: Robotic Platform for Locomotion and Manipulation of Lightweight Space Structures," in *AIAA SciTech*, (Grapevine, TX), 2017.

[8] W. Langford, A. Ghassaei, and N. Gershenfeld, "Automated Assembly of Electronic Digital Materials," in *ASME MSEC*, (Blacksburg, VA), pp. 1–10, 2016.

[9] R. MacCurdy, a. McNicoll, and H. Lipson, "Bitblox: Printable digital materials for electromechanical machines," *The International Journal of Robotics Research*, jul 2014.

[10] J. P. Whitney, P. S. Sreetharan, K. Y. Ma, and R. J. Wood, "Pop-up book MEMS," *Journal of Micromechanics and Microengineering*, vol. 21, no. 11, p. 115021, 2011.

[11] R. J. Wood, S. Avadhanula, R. Sahai, E. Steltz, and R. S. Fearing, "Microrobot Design Using Fiber Reinforced Composites," *Journal of Mechanical Design*, vol. 130, no. 5, p. 052304, 2008.

[12] N. Doshi, B. Goldberg, R. Sahai, N. Jafferis, D. Aukes, R. J. Wood, and J. A. Paulson, "Model driven design for flexure-based Microrobots," in *IEEE International Conference on Intelligent Robots and Systems*, vol. 2015-Decem, pp. 4119–4126, 2015.

[13] R. Wood, E. Steltz, and R. Fearing, "Optimal energy density piezoelectric bending actuators," *Sensors and Actuators A: Physical*, vol. 119, no. October 2004, pp. 476–488, 2005.

[14] A. P. Gerratt, B. Balakrisnan, I. Penskiy, and S. Bergbreiter, "Dielectric elastomer actuators fabricated using a micro-molding process," *Smart Materials and Structures*, vol. 23, p. 055004, may 2014.

[15] N. J. Kohut, A. M. Hoover, K. Y. Ma, S. S. Baek, and R. S. Fearing, "MEDIC: A legged millirobot utilizing novel obstacle traversal," *Proceedings - IEEE International Conference on Robotics and Automation*, pp. 802–808, 2011.

[16] B. Goldberg, M. Karpelson, O. Ozcan, and R. J. Wood, "Planar fabrication of a mesoscale voice coil actuator," *2014 IEEE International Conference on Robotics and Automation (ICRA)*, pp. 6319–6325, 2014.

[17] W. S. N. Trimmer, "Microrobots and Micromechanical Systems," *Sensors and Actuators*, vol. 19, no. 3, pp. 267–287, 1989.

[18] "Fully Automatic Hot Air Coil Winding Machine."

[19] D. C. Hanselman, *Brushless permanent magnet motor design*. 2006.

[20] C.-S. Liu and P. D. Lin, "Miniaturized auto-focusing VCM actuator with zero holding current," *Optics Express*, vol. 17, no. 12, p. 9754, 2009.

[21] M. Salerno, A. Firouzeh, and J. Paik, "A Low Profile Electromagnetic Actuator Design and Model for an Origami Parallel Platform," *Journal of Mechanisms and Robotics*, vol. 9, no. 4, p. 041005, 2017.

[22] B. H. Shin and S. Y. Lee, "Micro mobile robots using electromagnetic oscillatory actuator," *Proceedings of the IEEE RAS and EMBS International Conference on Biomedical Robotics and Biomechatronics*, pp. 575–580, 2012.

[23] "H2W NCC10-15-027-1RC."

[24] "Moticont LVCM-010-013-01."

[25] P. A. York, S. Member, R. J. Wood, and S. Member, "A geometrically-amplified in-plane piezoelectric actuator for mesoscale robotic systems," pp. 1263–1268, 2017.

[26] R. Yeh, S. Hollar, and K. S. J. Pister, "Single mask, large force, and large displacement electrostatic linear inchworm motors," *Journal of Microelectromechanical Systems*, vol. 11, no. 4, pp. 330–336, 2002.

[27] E. W. Schaler, L. Jiang, C. Lee, and R. S. Fearing, "Bidirectional, Thin-Film Repulsive-/Attractive-Force Electrostatic Actuators for a Crawling Milli-Robot," *MARSS 2018 (to appear)*, pp. 1–8, 2018.

[28] R. Merry, R. Van De Molengraft, and M. Steinbuch, "Modeling of a walking piezo actuator," *Sensors and Actuators, A: Physical*, 2010.

[29] Physikinstrumente, "Piezo Walk Piezo Motors," 2018.

[30] K. Spanner and B. Koc, "Piezoelectric Motors, an Overview," *Actuators*, vol. 5, no. 1, p. 6, 2016.

[31] R. Malka, A. L. Desbiens, Y. Chen, and R. J. Wood, "Principles of microscale flexure hinge design for enhanced endurance," *IEEE International Conference on Intelligent Robots and Systems*, no. Iros, pp. 2879–2885, 2014.

[32] C. E. Shannon, "A symbolic analysis of relay and switching circuits," 1938.